JURNAL SAINS MATERI INDONESIA (JUSAMI)
ISSN: 1411-1098 (print), 2614-087X (online)
VOL. 27, ISSUE 1 2025
DOI: https://doi.org/10.55981/jsmi.2025.9207

ORIGINAL ARTICLE

Binary Composite of Chitosan-Derived Porous Carbon/PANI for High Capacitance Performance of Supercapacitors

K. A. Gala[1,2], H. Gurning[1,2], I. Prasetyo[1,2] and T. Ariyanto[1,2*]

[1]Department of Chemical Engineering, Faculty of Engineering, Universitas Gadjah Mada, Yogyakarta, Indonesia
[2]Carbon Material Research Group, Department of Chemical Engineering, Faculty of Engineering, Universitas Gadjah Mada, Yogyakarta, Indonesia

ABSTRACT – The study of carbonaceous electrode materials for supercapacitors is expanding and remains challenging. Chitosan is one of the many biomasses found in nature that can be converted into porous carbon for electrode materials in supercapacitors. Despite having a high specific surface area and good chemical stability, porous carbons have a limitation of specific capacitance. On the other hand, polyaniline (PANI), a conductor polymer, typically exhibits high specific capacitance but has low stability. Thus, a binary nanocomposite of chitosan-derived porous carbon (CCS) and PANI is suggested to obtain an optimal performance. Porous carbon was produced from chitosan through two steps: (i) hydrothermal carbonization; (ii) chemical activation using steam at a temperature of 800 °C for 2 hours. The CCS was then oxidized with diluted H2O2 to increase surface wettability. Binary nanocomposites were produced by a nanocompositing method of in situ polymerization of PANI with a variation of 5% (CCS/PANI5%), 10% (CCS/PANI10%), and 15% (CCS/PANI15%). The materials were characterized by scanning electron microscopy–energy dispersive X-ray (SEM-EDX), Fourier-transform infrared (FTIR), N2-sorption analysis, and thermogravimetric analysis (TGA). Meanwhile, electrochemical tests were performed using a three-electrode method to obtain cyclic voltammetry and the capacitance of each sample. The N2-sorption analysis showed that the surface area of samples CCS, CCS/PANI5%, CCS/PANI10%, and CCS/PANI15% are 1305 m2.g-1, 430 m2.g-1, 333 m2.g-1, and 238 m2.g-1, respectively. SEM-EDX, FTIR, and TGA proved that PANI is loaded in the carbon surface. From the electrochemical tests conducted at a scan rate of 5 $mV.s^{-1}$, the specific capacitance values for the samples CCS, PANI, CCS/PANI5%, CCS/PANI10%, and CCS/PANI15% were determined to be 220.27 $F.g^{-1}$, 143.81 $F.g^{-1}$, 330.42 $F.g^{-1}$, 434.73 $F.g^{-1}$, and 391.27 $F.g^{-1}$, respectively. The CCS/PANI10% sample exhibited the highest specific capacitance of 434.73 $F.g^{-1}$, corresponding to an energy density of 86.9 $Wh.kg^{-1}$ and a power density of 1.3 $kW.kg^{-1}$. These significant enhancements in specific capacitance underscore the effectiveness of the nanocomposite approach and highlight its potential for improving electrode performance. As a result, the chitosan-based porous carbon and polyaniline nanocomposite developed in this study is a promising candidate for supercapacitor electrode materials.

ARTICLE HISTORY
Received: 27 Jan 2025
Revised: 05 Mar 2025
Accepted: 14 Mar 2025

KEYWORDS
Supercapacitor
Nanocomposite
Porous carbon
Chitosan
Polyaniline

INTRODUCTION

Supercapacitors have gained significant attention in academic and industrial fields due to their capacity to quickly charge, long cycle life, and high power density [1], [2]. Because of these desirable features, they may be used in a variety of settings, including as smart grids, hybrid electric cars, and portable gadgets [3]. Two categories of supercapacitors can be distinguished by their working mechanisms: electrical double-layer capacitors (EDLC) [4], which use electrostatic charges between the electrolyte and electrode surface to store energy, and redox pseudocapacitors, which typically use transition metal oxides and conducting polymers to facilitate rapid energy transfer via redox reactions at the electrode surface [5]. Despite their advantages, supercapacitors still face a limitation of having lower energy storage capacity compared to batteries [6]. Enhancing energy storage without compromising high performance has been a long-standing goal in advanced supercapacitor development. As a result, combining electrode materials that possess both EDLC and pseudocapacitor properties has been investigated to improve their overall performance [7].

A major factor affecting the electrochemical performance of supercapacitors is the electrode material selection. Currently, porous carbons are considered one of the most promising electrode materials because of their high physicochemical stability, low cost, affordability, and exceptional conductivity [8]. Porous carbon can be created from carbon precursors, either sourced from biobased materials [9] or through the synthesis of polymeric materials [10]. Chitosan, a renewable natural biomass, is an appealing raw material for producing carbon due to its low price and

*CORRESPONDING AUTHOR | T. Ariyanto | ✉ teguh.ariyanto@mail.ugm.ac.id

widely recognized extraction techniques from chitin [11]. Furthermore, amine groups in chitosan naturally integrate nitrogen functionalities into the carbon framework, contributing to high pseudocapacitance through a redox reaction [12]. Another commonly used electrode material is conducting polymers, with polyaniline (PANI) being a popular choice for supercapacitors due to its high pseudocapacitance, low density, affordability, and eco-friendliness. However, it has poor cycling stability [13]. While PANI electrodes provide better specific capacity than porous carbon, porous carbon offers a long cycle life.

Previous studies have investigated the development of activated carbon derived from chitosan. Activated carbon can be produced through a series of processes involving hydrothermal treatment and chemical activation. A study by Huang et al. synthesized porous carbon from chitosan via chemical activation using kalium hydroxide (KOH) [9]. However, chemical activation with KOH requires significant precautions and involves relatively high costs. Thus, there is a need for safer and more cost-effective alternatives to KOH. Furthermore, in efforts to enhance specific capacitance, several studies have explored the combination of bio-based activated carbon with the conducting polymer polyaniline (PANI) [7], [14], [15]. These studies have demonstrated that doping activated carbon with PANI enhances its conductivity.

Therefore, this work focuses on developing a binary nanocomposite that combines porous carbon derived from chitosan and PANI to create an electrode material with high specific capacity and improved cycle life. The proposed production pathway aims to excel in electrochemical performance and offer economic advantages by utilizing readily available chitosan and employing cost-effective processes. Additionally, this study seeks to identify the optimal formulation of the carbon chitosan and PANI to produce a superior nanocomposite for supercapacitor applications.

EXPERIMENTAL METHOD

Synthesis of Chitosan-Activated Carbon (CCS)

The two basic processes that chitosan goes through to create activated carbon are hydrothermal carbonization and chemical activation. In the hydrothermal process, chitosan in flake form was mixed with 0.1 M acetic acid at a mass ratio 1:10 between chitosan and solution. Acetic acid acts as an organic catalyst capable of naturally lowering the pH, accelerating the decomposition reaction. However, excessive addition of acetic acid can reduce the yield of carbonized solids [16]. A concentration of 0.1 M acetic acid with a chitosan-to-solution ratio of 1:10 was selected, as previous research demonstrated that this composition produces an optimal amount of hydrochar [17]. Afterwards, the mixture of chitosan and acetic acid was transferred to an autoclave and tightly sealed. Before heating, the autoclave was flushed with nitrogen gas to remove oxygen in the empty space and increase the pressure to 15 bar. The heating process was conducted at 250 °C for 14 hours. Following the heating procedure, the autoclave was set aside to naturally cool overnight, and the formed mixture was vacuum filtered and washed. Subsequently, the solid was dried in an oven for 24 hours at 100 °C, resulting in chitosan hydrochar.

The formed chitosan hydrochar will then undergo chemical activation through partial gasification using steam. This process was performed in a furnace with activation at 800 °C for 120 minutes with a constant steam and nitrogen gas flow. A 30-minute holding time was applied when the furnace reached 100 °C to optimize the removal of any remaining moisture in the hydrochar. The heating and cooling processes were done at a ramp rate of 2 °C/min. The result of this chemical activation was chitosan-activated carbon (CCS). Fresh CCS from the furnace was in granular form, so it was ground to 400 mesh to produce uniform CCS powder.

Synthesis of Binary Nanocomposite CCS/PANI

The preparation of binary CCS/polyaniline (PANI) nanocomposites involved the in-situ polymerization of aniline within the pores of CCS. The materials required for this process were 15% hydrogen peroxide (H2O2), aniline, ammonium persulfate (APS), 1 M hydrochloric acid (HCl), and acetone. All materials were obtained from Merck with a dilution with aquadest, if necessary, to obtain a suitable concentration. The process began with the oxidation of CCS by 15% H2O2 for 30 minutes. H_2O_2 is expected to enhance the wettability of carbon [18]. The mixture was then vacuum-filtered, and the cake was dried in an oven at 60 °C for 6 hours. The oxidized CCS was then weighed to 5 grams and placed into a reactor set at 0–5 °C with an aniline solution in 1 M HCl. Aniline serves as a monomer that undergoes polymerization to form polyaniline. The polymerization reaction of aniline is optimized under acidic conditions; therefore, 1 M HCl solution is added as an acid catalyst [17]. In addition, the polymerization reaction in polyaniline synthesis is an exothermic process, necessitating temperature control within the reactor by circulating ethanol as a cooling fluid. A low polymerization reaction temperature of 0–5°C is chosen to obtain polyaniline with high crystallinity. At low temperatures, the polymerization reaction proceeds slowly, allowing for the formation of a more well-defined crystalline structure, preventing polymer degradation, and avoiding a runaway reaction that could lead to undesirable products. Furthermore, a low polymerization temperature increases the number of covalent bonds formed, resulting in more stable polyaniline [19]. The amount of aniline added corresponds to the predetermined sample variations, which are 5%, 10%, and 15% relative to the mass of CCS. The study variation was limited to below 15% PANI addition, as previous research has shown that adding more than 15% PANI causes pore clogging in the carbon structure [20]. A mixture of 1 M HCl and APS solution was dripped into the reactor containing CCS and aniline to initiate the polymerization, with APS acting as the oxidizing initiator. The polymerization reaction lasts for 4 hours. The success of the polymerization process is indicated by a dark green colour change, signifying the formation of polyaniline in the emeraldine salt form [19]. The resulting CCS/PANI nanocomposite was filtered and rinsed using 1 M HCl and acetone. Rinsing with 1 M HCl aims to produce emeraldine salt-type polyaniline containing protonated amine

groups. These groups carry positive ions that attract negative ions, resulting in ionic bonds. Meanwhile, acetone is used to dissolve non-polymeric bonds in the polyaniline material, leaving only the main polymeric bonds, namely, benzenoid and quinoid groups [21]. The resulting polyaniline is then dried in a desiccator for 24 hours, followed by oven drying at 60 °C for 4 hours.

Characterization of Materials

The main material characterizations included morphology, pore structure, functional group characterizations, and thermal stability testing. The morphology of the nanocomposites was observed using scanning electron microscopy equipped with an energy-dispersive X-ray spectrometer (SEM-EDX). The characterization of the material pore structure was performed through nitrogen sorption using a Quantachrome NOVA 2000 equipment. The specific surface area was analyzed using Brunauer-Emmett-Teller (BET) methods. On the other hand, functional group characterizations were examined using Nicolet Avatar 360 Fourier-transform infrared (FTIR) equipment. Analysis using this method resulted in a pattern with peaks that corresponded with certain crystalline microstructures and functional groups. Furthermore, thermal stability was tested using thermogravimetric analysis (Linseis PT1000, Germany) under nitrogen atmosphere.

Electrochemical Measurement

The three-electrode system was used to determine the electrochemical measurement of a material-specific capacitance. The nanocomposite results from the CCS/PANI synthesis process were used as the working electrode material, platinum (Pt) as the counter electrode, and silver/silver chloride (Ag/AgCl) as the reference electrode (3 M kalium chloride (KCl) solution). The nanocomposite sample was weighed at 10 mg to set up the working electrode. Subsequently, the sample was mixed with 20 µL of Nafion 117 and 1 mL of isopropanol. Nafion 117 was used as a binder, while isopropanol served as a volatile solvent [22]. The resulting mixture was treated with sonication to ensure the nanocomposite sample was fully dispersed before being used on the working electrode. The electrolyte used during the electrochemical measurement process was a 1 M sulfuric acid (H2SO4) solution at an ambient temperature of 30 °C. The three-electrode measuring system was completed with the arrangement of the 1 M H2SO4 solution electrolyte, Pt counter electrode, and Ag/AgCl reference electrode. Using cyclic voltammetry techniques with a potential window range of -0.40 V to 0.80 V and a scan rate of 5, 10, 25, 50, 100 mV.s-1, the capacitance of the material was determined.

RESULT AND DISCUSSION

Materials Characteristic

Figure 1 (a) shows that the obtained chitosan-derived porous carbon (CCS) exhibits an irregular cavity morphology as seen in the scanning electron microscopy (SEM) images at the same magnification. These irregular cavities vary in size. In Figure 1 (b), the morphology of polyaniline appears to be agglomerated and layered. Combining the two materials, CCS and polyaniline (PANI), into CCS/PANI5% and CCS/PANI10% nanocomposite samples shows significant results, as seen in Figure 1 (c) and Figure 1 (d), respectively. As the mass percentage of PANI impregnated into the carbon increases, the carbon pores become more blocked compared to CCS in Figure 1 (a). Another related study by Chen et al. on synthesizing polyaniline/sugarcane bagasse-derived biocarbon nanocomposites with varying PANI content exhibited similar behavior [14]. The study showed SEM images that PANI nanoparticles gradually covered the clean surface of pristine activated carbon as the mass ratio of PANI to activated carbon increased. The energy-dispersive X-ray spectrometer (EDX) mapping characterization results of the nanocomposites in Table 1 further support this. An increase in the % nitrogen (N) element, characteristic of polyaniline, is observed on the surface of the samples from CCS/PANI5% to CCS/PANI10%. The decrease in the % carbon element from CCS/PANI5% to CCS/PANI10% samples indicates that the carbon visible on the surface is increasingly covered by other substances, in this case, polyaniline. This phenomenon may significantly impact the electrochemical performance of the nanocomposite.

Table 1. EDX mapping of the sample element result

Sample	Element (%)			
	C	O	N	Cl
CCS	77.79	20.95	1.26	-
PANI	60.71	10.12	26.75	2.42
CCS/PANI5%	60.45	21.55	12.02	5.98
CCS/PANI10%	59.56	21.29	15.45	3.70

To analyze the pore structure, an N2-sorption analysis was performed. The nitrogen adsorption and desorption isotherms are displayed in Figure 2 (a). The isotherms revealed that the nanocomposite materials exhibit a type IB isotherm, as per the International Union of Pure and Applied Chemistry (IUPAC) classification, indicating that they contain a large number of micropores with a wide size range, as well as mesopores [23]. The presence of mesopores is shown by an increase in the volume of nitrogen adsorbed at higher relative pressures (>0.2 P/Po). Additionally, Figure 2 (a) demonstrates that among CCS, CCS/PANI5%, CCS/PANI10%, and CCS/PANI15%, CCS has the highest nitrogen adsorption capacity. The introduction of PANI decreases the amount of nitrogen absorbed, with a greater reduction seen as more PANI is impregnated into the nanocomposites.

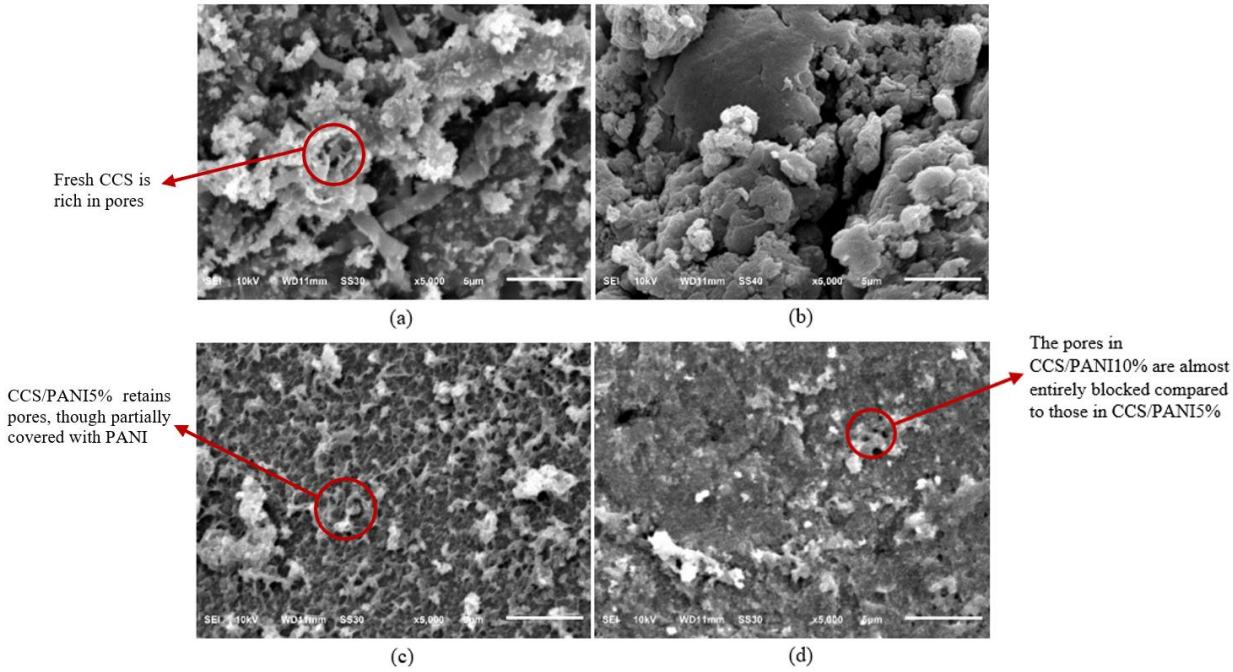

Figure 1. SEM image of: (a) CCS, (b) PANI, (c) CCS/PANI5%, and (d) CCS/PANI10%

Figure 2 (b) further confirms that both micropores and mesopores are present in CCS and the nanocomposites, with the most frequent pore diameters within 1–1.5 nm (micropores) and 2.5–3 nm (mesopores). As shown in Figure 2 (b), the number of micropores and mesopores decreases as more PANI is impregnated into CCS due to PANI either filling or blocking the pores. The reduction in pore size due to PANI impregnation is also supported by the specific surface area (SSA) data in Table 2. Maxsorb was included as an additional reference because it has a high surface area of activated carbon, with a measured surface area of 2643.67 $m^2.g$-1. This value is close to the specific surface area reported in a previous study [24], which stated a value of 2805 $m^2.g$-1. The surface area values based on Table 2, from highest to lowest, are as follows: Maxsorb > CCS > CCS/PANI5% > CCS/PANI10% > CCS/PANI15%. PANI is a conductive polymer with a relatively low specific surface area [7]. Consequently, compared to other samples, PANI exhibits the lowest specific surface area with a value of 35.43 $m^2.g$-1. Adding PANI to CCS reduces specific surface area, which can be attributed to two main factors: the clogging of pores and an increase in mass. PANI's blockage of CCS pores primarily causes a reduction in specific surface area. This phenomenon is particularly evident in the significant decrease in specific surface area observed in the CCS/PANI5% compared to CCS. The specific surface area decreased from 1305.48 $m^2.g$-1 in CCS to 430.80 $m^2.g$-1 in CCS/PANI5%. Additionally, the increase in PANI mass within CCS, while maintaining a constant total surface area, also leads to a decrease in specific surface area since specific surface area is calculated as the ratio of the total surface area to the sample mass. The reduction by this factor occurs gradually, as observed in the sample sequence: CCS/PANI5% > CCS/PANI10% > CCS/PANI15%. The specific surface area values for these samples are 430.80 $m^2.g$-1, 333.58 $m^2.g$-1, and 238.42 $m^2.g$-1, respectively.

Table 2. Summarized pore characteristics of the sample

Sample	Specific Surface Area ($m^2.g^{-1}$)	Mean Pore Diameter (nm)	Micropore Volume ($cm^3.g^{-1}$)	Total Pore Volume ($cm^3.g^{-1}$)
CCS	1305.48	2.58	0.54	0.84
CCS/PANI5%	430.80	8.39	0.01	0.90
CCS/PANI10%	333.58	3.31	0.09	0.28
CCS/PANI15%	238.42	3.61	0.06	0.22
PANI	35.43	17.79	-	0.16
Maxsorb	2643.67	2.19	0.83	1.45

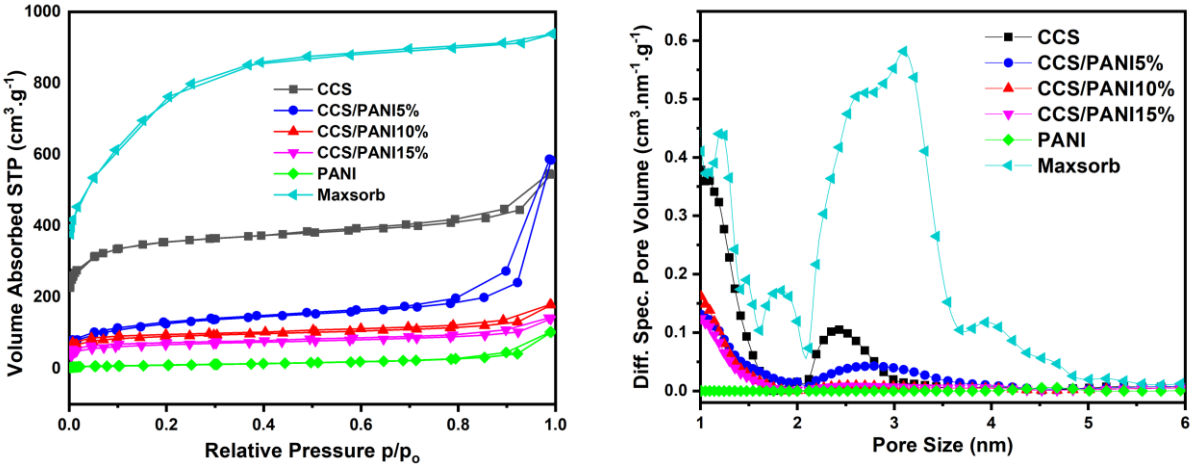

Figure 2. (a) Nitrogen adsorption-desorption isotherms and (b) pore size distributions of ternary composite of CCS, PANI, binary composites, and Maxsorb

The Fourier-transform infrared (FTIR) spectra of the materials are shown in Figure 3. The FTIR spectrum of CCS material is indicated by wavelength at 3400 cm^{-1}, a crucial marker that signifies the presence of amine or -OH groups corresponding to the stretching of hydroxyl groups (-OH) resulting from the pre-treatment of porous CCS material with a 15% hydrogen peroxide (H2O2) solution, aimed at improving the wettability of the carbon surface [18]. The peak at 1612 cm^{-1}, due to C=C stretching vibrations in the aromatic ring or deformation vibrations of -NH, is another significant feature [25]. The spectra between 1250 and 1020 cm^{-1} indicate the presence of C-N, representing amine groups on the CCS backbone [25]. Meanwhile, the absorption band at 900 cm^{-1} signifies the presence of C=C groups in CCS [25], [26].

The FTIR absorption bands for PANI are identified at wavelengths of 3400 cm^{-1}, 1600 cm^{-1}, 1500 cm^{-1}, 1300 cm^{-1}, 1120 cm^{-1}, 800 cm^{-1}, and 600 cm^{-1}. The 3400 cm^{-1} wavelength indicates the presence of amine bonds [26]. In the spectra at wavelengths of 1500 cm^{-1} and 1600 cm^{-1}, peaks confirm the presence of benzenoid and quinoid rings [26]. Figure 3 shows that the intensity of the benzenoid spectra is higher than that of the quinoid spectra. The intensity ratio of the peaks at these bands (I1600/I1500) serves as a qualitative indicator of the oxidation state of the polymer. As expected, the peak at 1600 cm^{-1} is stronger than the peak at 1500 cm^{-1}, with a ratio of ~0.6, indicating the formation of the emeraldine base of polyaniline (PANI) [27]. The peak associated with PANI's conductivity is located at the wavelength of 1150 cm^{-1}, confirming the presence of -NH+ bonds, which measure the degree of electron delocalization [25]. Additionally, there is a wavelength range between 850-550 cm^{-1}, indicating the presence of C-Cl bonds resulting from using hydrogen chloride (HCl) as a catalyst in PANI synthesis [28].

The FTIR spectrum of the CCS/PANI10% nanocomposite, when compared to the PANI spectrum, does not show significant differences. The distinction lies in the composite spectrum, where a slightly different intensity ratio is observed between 1500 cm^{-1} and 1600 cm^{-1}, as the data reveal a higher quinoid content compared to benzenoid. This intriguing finding indicates that the CCS/PANI interaction plays a crucial role in stabilizing the quinoid ring structure. This interaction is attributed to the aromatic structure of PANI, which is generally known to strongly interact with the basal planes of carbon surfaces through π-bond stacking. The spectrum at 1300 cm^{-1} shows the presence of C-N bonds related to electron delocalization. Thus, it can be concluded that HCl-doped polyaniline has been successfully impregnated in the CCS, forming a nanocomposite [7], [26].

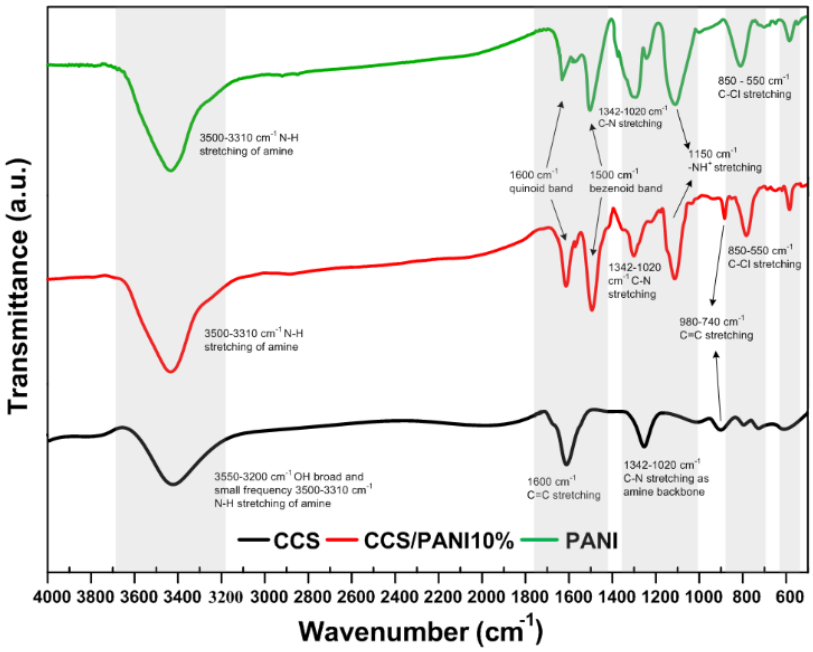

Figure 3. FTIR spectra of CCS, PANI, binary composites

The outcomes of the thermogravimetric analysis (TGA) are displayed in Figure 4. All three samples—CCS, CCS/PANI5%, and CCS/PANI10%—experienced a drastic weight loss in the temperature range of 30–120 °C. This indicates the removal of moisture from the samples [29], [30]. This reflects that CCS has a higher hydrophilic character compared to the binary composite. Then, in the temperature range of 120–400 °C, a gradual weight loss was attributed to eliminating volatile substances and decomposition of PANI in the samples. PANI undergoes thermo-oxidative breakdown, producing a variety of degradation products, including methane, ammonia, and aniline [31]. For CCS, a relatively plateau at 120°C–400 °C can confirm that no organic material of aniline is being impregnated. After reaching 400 °C, a significant mass reduction occurred again as the volatile substances had fully decomposed, leaving only carbon (C). The reaction between 500–700 °C involves the combustion of the carbon material with oxygenated groups of the CCS.

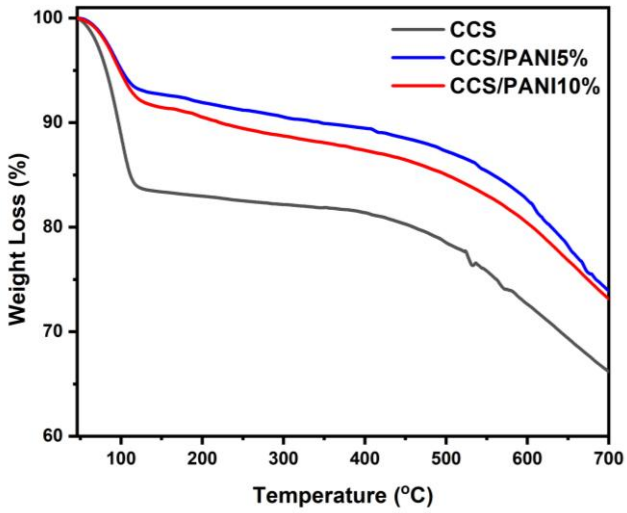

Figure 4. TGA of CCS and binary composites

Electrochemical Properties

A cyclic voltammetry (CV) graph can identify the type of supercapacitors based on size and shape. The capacitance value can be determined from the area generated in the CV graph. In Figure 5, the CV graph has distinct CV shapes for each material at a scan rate of 5 $mV.s^{-1}$. The CCS with a capacitance of 220.27 $F.g^{-1}$ exhibits a rectangular-like shape with a slightly bulky center in the curve. The rectangular-like shape can be explained by the fact that carbon stores electrical charges due to electrostatic forces between the accumulation of ions and electric charges, forming a double-layer capacitance [20]. Bulk in the CCS CV graph could indicate the presence of a heteroatom doping effect, particularly the nitrogen content in functional groups, which may contribute to the increase in capacitance [32]. On the other hand, PANI, with a capacitance of 143.81 $F.g^{-1}$, creates a profile featuring peaks at both the top and bottom parts. The peak at the top part signifies an oxidation reaction, whereas the one at the bottom indicates a reduction reaction [33]. These peaks signify the occurrence of Faradaic redox reactions, which are characteristic of pseudocapacitors [34]. Meanwhile, the three binary nanocomposites in Figure 5 show similar curves with increasingly higher peaks. The curved shape of the binary nanocomposites is significantly different from that of CCS due to the impregnation of PANI into the pores of CCS, which alters the shape of the CV graph. Based on the CV graph area analysis results, the capacitance values for CCS/PANI5%, CCS/PANI10%, and CCS/PANI15% are 330.42 $F.g^{-1}$, 434.73 $F.g^{-1}$, and 391.27 $F.g^{-1}$, respectively. The optimum capacitance value is found in CCS/PANI10%. This indicates that in CCS/PANI15%, the excess addition of PANI leads to pore blocking in the CCS pores. As a result, the capacitance value for CCS/PANI15% is not higher than that of CCS/PANI10%. The specific capacitance results in this research surpass previous research on another binary composite of carbon/PANI [7].

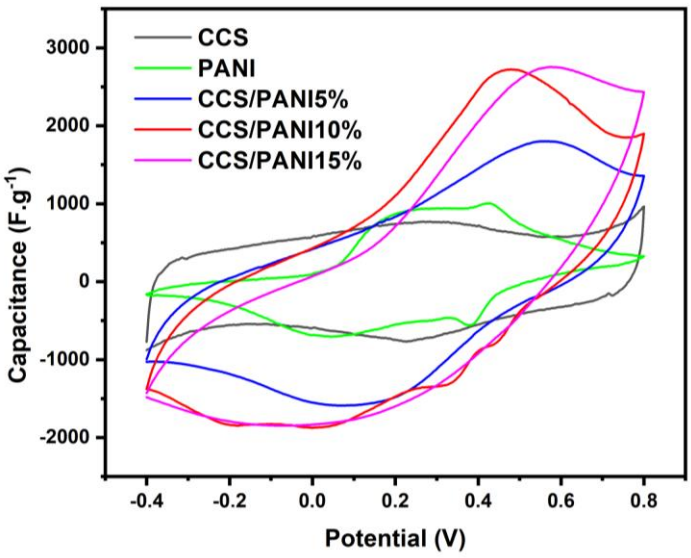

Figure 5. Cyclic voltammetry of CCS, PANI, and binary composites at 5 $mV.s^{-1}$

An inverse relation between specific capacitance and scanning rate is shown in Figure 6. CV tends to yield higher capacitance at low scanning rates and vice versa; CV tends to yield lower capacitance at high scanning rates. Lower scanning rates are thought to increase capacitance by facilitating more even electrolyte penetration into the pores and improved electrolyte-interface material interaction [35]. While at a higher scan rate, the electrode and electrolyte are in contact for shorter periods of time, resulting in less charge being stored on the electrode surface [36]. The ohmic resistance of electrolyte migration in the pores rises with an increase in scan rate, which decreases measured capacitance [37]. The linear relationship between the capacitance and scan rate suggests that the transport of ions is a diffusion-controlled process [35]. The relationship between specific capacitance and current density in Figure 6 exhibits a trend similar to the study on the fabrication of polyaniline/sugarcane bagasse-derived biocarbon nanocomposites conducted by Chen et al. [14].

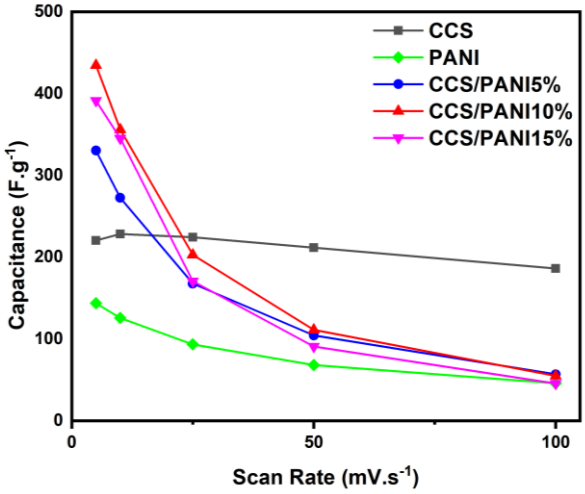

Figure 6. Capacitance vs. scan rate of CCS, PANI, and binary composites

Another indicator that can measure the performance of a supercapacitor is the Ragone plot, shown in Figure 7. The Ragone plot examines the relation between energy density and power density. The CCS/PANI10% nanocomposite has the highest energy density value of 86.9 $Wh.kg^{-1}$ with a power density of 1.3 $kW.kg^{-1}$. These results surpass those of the study by Chen et al. [14], with a maximum energy density of 27.29 $Wh.kg^{-1}$ at a power density of 0.8 $kW.kg^{-1}$. CCS/PANI5% and CCS/PANI15% have lower energy densities, at 66.1 $Wh.kg^{-1}$ and 78.3 $Wh.kg^{-1}$, respectively. It is known that the optimum specific capacitance is achieved by CCS/PANI10% because, in CCS/PANI15%, pore blocking of polyaniline in the CCS occurs, resulting in a reduction in both capacitance and energy density. The reduction in energy density increases with the higher PANI content in the CCS. The energy density reductions for CCS/PANI5%, CCS/PANI10%, and CCS/PANI15% are 82.78%, 87.33%, and 88.35%, respectively. Additionally, the energy density reductions for CCS and PANI are 15.48% and 68.08%, respectively. However, the highest power density achieved by CCS and PANI is not very high, at 0.7 $kW.kg^{-1}$ and 0.4 $kW.kg^{-1}$, respectively. The CCS/PANI10% material demonstrates good performance as a supercapacitor electrode, considering the capacitance value, energy density, and power density.

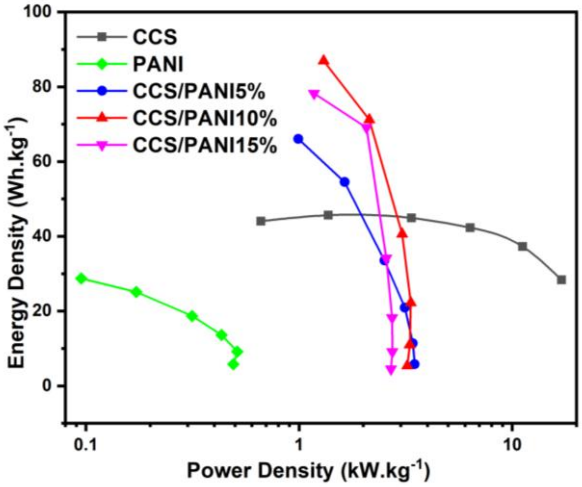

Figure 7. Ragone plot of CCS, PANI, and binary composites

CONCLUSION

The binary nanocomposite chitosan-derived porous carbon/polyaniline (CCS/PANI) was successfully synthesized through a sequence of processes, including the hydrothermal carbonization of chitosan, chemical activation using steam, and in situ polymerization of polyaniline. The resulting nanocomposite was tested as a supercapacitor electrode

material and underwent characterization via scanning electron microscopy–energy dispersive X-ray (SEM-EDX), Fourier-transform infrared (FTIR), N2-sorption, and Thermogravimetric analysis TGA). Based on N2-sorption analysis, CCS produced through hydrothermal carbonization and chemical activation exhibited a high surface area. Compared to CCS/PANI nanocomposites with varying PANI mass content, CCS possesses pristine pores that remain unfilled by PANI. As a result, CCS exhibits the highest specific surface area of 1305.48 $m^2.g^{-1}$. In the synthesized binary nanocomposite, PANI was loaded onto the carbon derived from chitosan, as evidenced by SEM and FTIR analysis. The SEM images from this study show the phenomenon of PANI pores being progressively blocked by CCS as the PANI mass increases. Meanwhile, the FTIR results confirm the presence of PANI in the emeraldine salt form within the CCS/PANI nanocomposites. The characteristic wavelengths at 1500 cm^{-1} and 1600 cm^{-1} correspond to the benzenoid and quinoid rings, which are distinctive features of PANI. Additionally, EDX mapping analysis confirmed the presence of nitrogen elements, a characteristic of PANI, distributed across the component's surface. The addition of PANI caused a change in the thermal stability of the electrode material, which was tested using the TGA analysis method. Three variations of PANI content in CCS were made: CCS/PANI5%, CCS/PANI10%, and CCS/PANI15%. Among these variations, the best supercapacitor electrode performance was shown by CCS/PANI10%, with a specific capacitance of 434 F.g-1. This binary nanocomposite combination showcases an energy density of 86.9 Wh.kg-1 and a power density of 1.3 kW.kg-1. Contrary to expectations, the specific capacitance of CCS/PANI15% (391.27 $F.g^{-1}$) does not surpass CCS/PANI10%. This is due to the addition of 15% PANI, which exceeds the pore-loading capacity of CCS, resulting in significant pore blockage that adversely impacts the electrochemical performance of the nanocomposite. These findings highlight the importance of adjusting the PANI content to maximize the electrochemical performance of nanocomposite-based electrode materials.

ACKNOWLEDGEMENT

The authors would like to express their sincere gratitude to the Carbon Material Research Group, Universitas Gadjah Mada, for their invaluable support in conducting this research.

REFERENCES

[1] H. Rustamaji, T. Prakoso, H. Devianto, P. Widiatmoko, and I. Nurdin. “Design, Fabrication, and Testing of Supercapacitor Based On Nanocarbon Composite Material.” *ASEAN Journal of Chemical Engineering,* vol. 22, no. 1, pp. 19–32, 2022.

[2] M. Horn, J. MacLeod, M. Liu, J. Webb, and N. Motta. “Supercapacitors: A New Source of Power for Electric Cars?” *Economic Analysis and Policy*, vol. 61, pp. 93–103, 2019.

[3] L. Xie, G. Sun, F. Su, X. Guo, Q. Kong, X. Li, X. Huang, W. Song, K. Li, Lv. Chunxiang, and C. M. Chen. “Hierarchical Porous Carbon Microtubes Derived from Willow Catkins for Supercapacitor Applications.” *J Mater. Chem. A.*, vol. 4, pp. 1637–1646, 2016.

[4] W. Raza, F. Ali, N. Raza, Y. Luo, K. Hyun-Ki, J. Yang, S. Kumar, A. Mehmood, and E. E. Kwon. “Recent Advancements in Supercapacitor Technology.” *Nano Energy*, vol. 52, pp. 441–473, 2018.

[5] M. I. Fuady, R. Rochmadi, I. Prasetyo, and T. Ariyanto. “Surface-modified Carbon Synthesized from Palm Kernel Shell for Electric Double-Layer Capacitor Applications.” *Key Eng. Mater.*, vol. 884, pp. 423–429, 2021.

[6] A. González, E. Goikolea, J. A. Barrena, and R. Mysyk. “Review on Supercapacitors: Technologies and Materials.” *Renewable and sustainable energy reviews*, vol. 58, pp. 1189–1206, 2016.

[7] J. F. Wibowo, I. Prasetyo, and T. Ariyanto. “PANI/Porous Carbon Palm Kernel Shell via In Situ Polymerization Method for Supercapacitor Electrode.” *Solid State Phenom.*, vol. 345, pp. 123–130, 2023.

[8] X. He, N. Zhang, X. Shao, M. Wu, M. Yu, and J. Qiu. “A Layered-Template-Nanospace-Confinement Strategy for Production of Corrugated Graphene Nanosheets from Petroleum Pitch for Supercapacitors.” *Chem. Eng. J.*, vol. 297, pp. 121–127, 2016.

[9] J. Huang, Y. Liang, H. Hu, S. Liu, Y. Cai, H. Dong, M. Zheng, Y. Xiao, and Y. Liu. “Ultrahigh-Surface-Area Hierarchical Porous Carbon from Chitosan: Acetic Acid Mediated Efficient Synthesis and Its Application in Superior Supercapacitor.” *Material Chemistry A.*, vol. 5, pp. 24775–24781, 2017.

[10] T. Ariyanto, I. Prasetyo, and R. Rochmadi. “Pengaruh Struktur Pori terhadap Kapasitansi Elektroda Superkapasitor yang Dibuat dari Karbon Nanopori.” *REAKTOR*, vol.14, no. 1, pp. 25–32, 2012.

[11] P. Hao, Z. Zhao, Y. Leng, J. Tian, Y. Sang, R. I. Boughton, C. P. Wong, H. Liu, and B. Yang. “Graphene-Based Nitrogen Self-Doped Hierarchical Porous Carbon Aerogels Derived from Chitosan for High Performance Supercapacitors.” *Nano Energy*, vol. 15, pp. 9–23, 2015.

[12] X. Deng, B. Zhao, L. Zhu, and Z. Shao. “Molten Salt Synthesis of Nitrogen-Doped Carbon with Hierarchical Pore Structures for Use as High-Performance Electrodes in Supercapacitors.” *Carbon*, vol. 93, pp. 48–58, 2015.

[13] H. Zhou, X. Zhi, and H. J. Zhai. “A Facile Approach to Improve the Electrochemical Properties of Polyaniline-Carbon Nanotube Composite Electrodes for Highly Flexible Solid-State Supercapacitors.” *Int. J. Hydrogen Energy*, vol. 43, no. 39, pp. 18339–18348, 2018.

[14] J. Chen, J. Qiu, B. Wang, H. Feng, Y. Yu, and E. Sakai. “Polyaniline/Sugarcane Bagasse Derived Biocarbon Composite with Superior Performance in Supercapacitors.” *Journal of Electroanalytical Chemistry*, vol. 801, pp. 360–367, 2017.

[15] K. M. Vighnesha, Sandhya Shruthi, D.N. Sangeetha, and M. Selvakumar. “Synthesis and Characterization of Activated Carbon/Conducting Polymer Composite Electrode for Supercapacitor Application.” *J. Mater. Sci. Mater. Electron*, vol. 29, pp. 914–921, 2018.

[16] W. Yan, T. C. Acharjee, C. J. Coronella, and V. R. Vásquez.”Thermal Pretreatment of Lignocellulosic Biomass.” *Environmental Progress & Sustainable Energy*, vol. 28, no. 3, pp. 435–440, 2009.

[17] H. Gurning. “Preparasi Material Nanokomposit Karbon Berpori/Polianilin sebagai Amine-Rich Adsorbent untuk Penjerapan CO_2 dan Ion Fosfat dalam Air Limbah.” Thesis, Universitas Gadjah Mada, Yogyakarta, 2024.

[18] N. I. F. Mukti, T. Ariyanto, W. B. Sediawan, and I. Prasetyo. "Efficacy of Modified Carbon Molecular Sieve with Iron Oxides or Choline Chloride-Based Deep Eutectic Solvent for the Separation of CO_2/CH_4." *RSC Advances*, vol. 13, no. 33, pp. 23158–23168, 2023.

[19] J. Stejskaland R. G. Gilbert."Polyaniline. Preparation of a Conducting Polymer: (IUPAC Technical Report)." *Pure and Applied Chemistry*, vol. 74, no. 5, pp. 857–867, 2002.

[20] U. Islamia. "Preparasi Karakterisasi Terneri Nanokomposit Karbon/Fe_3O_4/PANI untuk Material Elektroda pada Superkapasitor." Thesis, Universitas Gadjah Mada, Yogyakarta, 2024.

[21] M. Beygisangchin, S. A. Rashid, S. Shafie, A. R. Sadrolhosseini, and H. N. Lim. "Preparations, Properties, and Applications of Polyaniline and Polyaniline Thin Films—A Review." *Polymers*, vol. 13, no. 12, pp. 2003, 2021.

[22] T. Ariyanto, B. Dyatkin, G. R. Zhang, A. Kern, Y. Gogotsi, and B. J. M. Etzold. "Synthesis of Carbon Core-Shell Pore Structure and Their Performance as Supercapacitors." *Microporous and Mesoporous Materials,* vol. 218, pp. 130–136, 2015.

[23] M. Thommes, K. Kaneko, A. V. Neimark, J. P. Olivier, F. Rodriguez-Reinoso, J. Rouquerol, and K. S. W. Sing. "Physisorption of Gases, with Special Reference to the Evaluation of Surface Area and Pore Size Distribution (IUPAC Technical Report)." *Pure and Applied Chemistry*, vol. 87, no. 9–10, pp. 1051–1069, 2015.

[24] S. Kayal and A. Chakraborty. "Activated Carbon (Type Maxsorb-III) and MIL-101(Cr) Metal Organic Framework Based Composite Adsorbent for Higher CH_4 Storage and CO_2 Capture." *Chemical Engineering Journal,* vol. *334*, pp. 780–788, 2018.

[25] S. Quillard, G. Louarn, S. Lefrant, and A.G. MacDiarmid. "Vibrational Analysis of Polyaniline: A Comparative Study of Leucomeraldine, Emeraldine, and Pernigraniline Bases." *Phys. Rev. B*, vol. 50, pp. 12496, 1994.

[26] H. Zengin, W. Zhou, J. Jin, R. Czerw, D. W. Smith, L. Echegoyen, D. L. Carroll, S. H. Foulger, and J. Ballato. "Carbon Nanotube Doped Polyaniline." *Advanced Materials*, 14, no. 20, 1480–1483, 2002.

[27] G. E. Asturias, A. G. MacDiarmind, R. P. McCall, and A.J. Epstein. "The Oxidation State of "Emeraldine" Base." *Synthesis Metals*, vol. 29, no. 1, pp. 157–162, 1989.

[28] M. Trchová, I. Šeděnková, E. Tobolková, and J. Stejskal. "FTIR Spectroscopic and Conductivity Study of the Thermal Degradation of Polyaniline Films." *Polymer Degradation and Stability*, vol. 86, no. 1, pp. 179–185, 2004.

[29] D. Zhu, Y. Wang, W. Lu, H. Zhang, Z. Song, D. Luo, L. Gan, M. Liu, and D. Sun. "A Novel Synthesis of Hierarchical Porous Carbons from Interpenetrating Polymer Networks for High Performance Supercapacitor Electrodes." *Carbon*, vol. 111, pp. 667–674, 2017.

[30] D. Maity, M. Manoharan, and R. T. R. Kumar. "Development of the PANI/MWCNT Nanocomposite-Based Fluorescent Sensor for Selective Detection of Aqueous Ammonia." *ACS Omega,* vol. 5, no. 15, pp. 8414–8422, 2020.

[31] P. C. Ramamurthy, A. M. Malshe, W. R. Harrell, R. V. Gregory, K. McGuire, and A. M. Rao. "Polyaniline/Single-Walled Carbon Nanotube Composite Electronic Devices." *Solid-State Electron*, vol. 48, pp. 2019–2024, 2004.

[32] Z. Li, Z. Xu, H. Wang, J. Ding, B. Zahiri, C. M. B. Holt, X. Tan, and D. Mitlin. "Colossal Pseudocapacitance in A High Functionality–High Surface Area Carbon Anode Doubles The Energy of An Asymmetric Supercapacitor." *Energy & Environmental Science*, vol. 7, no. 5, pp. 1708–1718, 2014.

[33] H. Wang, J. Lin, and Z. X. Shen. "Polyaniline (PANi) Based Electrode Materials for Energy Storage and Conversion." *J. Sci. Adv. Mater. Devices*, vol. 1, no. 3, pp. 225–255, 2016.

[34] H. Li, J. Wang, Q. Chu, Z. Wang, F. Zhang, and S. Wang. "Theoretical and Experimental Specific Capacitancec of Polyaniline in Sulfuric Acid." *Journal of Power Sources*, vol. 190, no. 2, pp. 578–586, 2009.

[35] N. Mishra, S. Shinde, R. Vishwakarma, S. Kadam, and M. Sharon. "MWCNTs Synthesized from Waste Polypropylene Plastics and Its Application in Supercapacitors." *AIP Conf*., 2013.

[36] C. Largeot, C. Portet, J. Chmiola, P. L. Taberna, Y. Gogotsi, and P. Simon. "Relation Between the Ion Size and Pore Size for An Electric Double-Layer Capacitor." *J. Am. Chem. Soc*., vol. 130, no. 9, pp. 2730–2731, 2008.

[37] H. Y. Liu, K. P. Wang, and H. Teng. "A Simplified Preparation of Mesoporous Carbon and the Examination of the Carbon Accessibility for Electric Double Layer Formation." *Carbon*, vol. 43, no. 3, pp. 559–566, 2005.